Echo Geometry of the Classical CHSH Ridge: Memory, Curvature, and Directional Susceptibility

Paper 2: The Memory Landscape

Kelly McRae

December 2025

Abstract

Paper 1 showed that a pair of deterministically coupled oscillators exhibits a well-defined CHSH landscape: a high-$|S|$ ridge at low noise and a sharp collapse boundary at $\sigma_c(K)$. Here we extend this analysis by resolving the *temporal structure* of CHSH correlations across the full (K, σ) plane. Using lag-resolved correlation decay, curvature, susceptibility, and angle-dependent scanning, we identify three robust regimes. (1) A trivial noise-dominated basin in which $|S| < 2$ and all memory measures vanish. (2) A structured intermediate band where $|S| > 2$ persists but long-lag memory has already collapsed, marked by a shallow mid-range enhancement in $\rho_S(\tau)$ and a complex pattern of positive and negative curvature. (3) A narrow ridge of strong instantaneous coherence in which $|S| \approx 2.8$ but temporal persistence remains extremely fragile. Across the entire domain we find a universal memory threshold $\sigma_{\text{mem}} \approx 0.002$, two orders of magnitude below the CHSH collapse curve, beyond which long-lag CHSH memory cannot be sustained for any choice of angles, confirming that memory collapse reflects intrinsic relative-phase dynamics rather than discretization or finite sampling.

We further treat the CHSH functional as a directional field by scanning across all measurement geometries. The resulting angle-resolved surfaces show that the optimal CHSH configuration twists under noise, exhibiting multiple susceptibility sign changes and a well-defined angle-flow structure. Evaluated at these optimal angles, long-lag memory still collapses at the universal threshold, confirming that temporal coherence is limited by intrinsic dynamics rather than geometry. Together, these results show that the CHSH ridge is a multi-layered temporal object whose instantaneous and lagged correlations are governed by distinct noise scales. This temporal decomposition provides the framework used in Paper 3 to analyze CHSH-like memory in small oscillator networks.

Contents

1 Introduction **3**
- 1.1 Motivation . . . 3
- 1.2 Background and Related Work . . . 3
- 1.3 Contributions . . . 3
- 1.4 Outline . . . 3

2 Methods **4**
- 2.1 Model . . . 4
- 2.2 Continuous-phase CHSH functional . . . 4
- 2.3 Temporal correlation and memory measures . . . 4
- 2.4 Directional susceptibility χ (formerly recursive susceptibility) . . . 5
- 2.5 Memory-collapse threshold . . . 5
- 2.6 Angle-resolved field geometry . . . 5
- 2.7 Software and reproducibility . . . 5

3 Results **5**
- 3.1 Universal noise threshold for temporal CHSH memory . . . 5
- 3.2 Memory curvature across the CHSH landscape . . . 7
- 3.3 Echo and susceptibility surfaces . . . 9
- 3.4 Synthesis: Three regimes of CHSH memory dynamics . . . 11
- 3.5 Angle-Resolved Geometry of the CHSH Field . . . 13

4 Discussion **14**

5 Conclusion **15**

1 Introduction

1.1 Motivation

Coupled phase oscillators provide a simple but expressive setting for studying CHSH-like correlations in classical dynamics. In Paper 1 we established that a pair of deterministically coupled oscillators produces a well-defined CHSH landscape: a high-$|S|$ ridge for sufficiently strong coupling and low noise, and a sharp collapse curve $\sigma_c(K)$ that separates high-$|S|$ from classical regimes. Yet that analysis treated the CHSH functional as a time-averaged quantity, collapsing the temporal dimension into a single statistic.

Here we restore that temporal dimension. By computing lag-resolved correlations across the full (K, σ) plane, we reveal the internal structure of the CHSH ridge: how $S(t)$ "remembers" itself at finite lags, how that memory degrades under noise, and whether the system's temporal coherence can survive when the instantaneous magnitude $|S|$ remains high.

1.2 Background and Related Work

The CHSH inequality [1] and its generalizations [2] have been extensively studied in the context of quantum foundations and information theory, building on Bell's original work [3]. Classical analogues of Bell-type correlations arise in a variety of dynamical systems, from coupled oscillators to chaotic maps, whenever continuous measurement parameters can be tuned to maximize correlations between subsystems. Following the classical Kuramoto framework [4, 5, 6], we adopt a minimal setting in which coupling strength and noise amplitude can be varied independently, allowing systematic exploration of the correlation landscape.

Previous work has focused primarily on instantaneous or time-averaged CHSH statistics. The temporal structure of correlations—how CHSH memory decays with lag, how curvature varies across parameter space, and how susceptibility responds to noise—has received less attention. This paper addresses that gap by introducing lag-resolved diagnostics that reveal the internal temporal organization of the CHSH ridge.

1.3 Contributions

The central finding is that instantaneous magnitude and temporal memory are governed by distinct noise scales. CHSH memory collapses at $\sigma_{\text{mem}} \approx 0.002$—roughly thirty times lower than the $|S|$-collapse curve $\sigma_c(K)$. This separation defines three robust regimes in the (K, σ) plane: (1) a noise-dominated basin where both $|S|$ and memory are trivial; (2) a structured intermediate band where $|S| > 2$ persists but long-lag memory has already vanished; and (3) a narrow ridge of maximal $|S|$ and non-zero memory. Throughout these regimes, the curvature and susceptibility of the CHSH memory field encode nontrivial temporal structure that cannot be read from the $|S|$ functional alone.

We further examine the CHSH functional as a directional field by scanning across all measurement geometries. This angle-resolved analysis shows that the optimal CHSH configuration twists under noise, with the susceptibility $\partial S^*/\partial\sigma$ changing sign multiple times as coupling and noise vary. Evaluated at these optimal angles, long-lag memory still collapses at σ_{mem}, confirming that the memory threshold arises from intrinsic dynamics rather than geometric artifact.

1.4 Outline

The paper is organized as follows. Section 2 defines the observables—echo strength $\rho_S(\tau)$, memory curvature, and susceptibility—and specifies the simulation and grid parameters. Section 3 presents results in five subsections: (3.1) the σ_{mem} threshold and regime separation; (3.2) the curvature surface and its sign structure; (3.3) echo and susceptibility surfaces; (3.4) synthesis of the three regimes; and (3.5) angle-resolved observer fields. Section 4 discusses implications for classical CHSH dynamics and

the coherence-memory distinction. The conclusion summarizes the framework and sets the stage for Paper 3, where we extend the analysis to small oscillator networks.

2 Methods

2.1 Model

The stochastic Kuramoto model is a canonical system in synchronization theory [4, 5, 6], making it a natural platform for exploring CHSH-like geometries. We study a pair of bidirectionally coupled phase oscillators governed by stochastic Kuramoto dynamics [4, 7],

$$\dot{\theta}_1 = \omega_1 + K\sin(\theta_2 - \theta_1) + \sigma\,\xi_1(t), \tag{1}$$
$$\dot{\theta}_2 = \omega_2 + K\sin(\theta_1 - \theta_2) + \sigma\,\xi_2(t), \tag{2}$$

where $(\theta_1, \theta_2) \in [0, 2\pi)$ are phases, K is coupling strength, σ is additive Gaussian noise amplitude, and $\xi_i(t)$ are independent Wiener processes with variance $2\,\mathrm{d}t$. Unless noted otherwise we set $\omega_1 = 1.0$, $\omega_2 = 1.0 + \Delta\omega$ with $\Delta\omega = 0.2$. Dynamics are integrated with the Euler–Maruyama method using timestep $\mathrm{d}t = 0.01$ for $T = 6 \times 10^5$ steps, with the first 3×10^5 discarded as transient.

We explore a rectangular grid in the (K, σ) plane. Coupling is sampled uniformly from $K \in [0.10, 1.00]$ in 19 steps; noise from $\sigma \in [0.00, 0.60]$ in 21 steps unless otherwise noted. Each configuration is repeated for 5 independent random seeds.

2.2 Continuous-phase CHSH functional

At each sampling time t we evaluate a continuous-phase version of the CHSH functional [1],

$$S(t) = E(a,b) - E(a,b') + E(a',b) + E(a',b'), \tag{3}$$

where a, a', b, b' are measurement angles and

$$E(x,y) = \cos(\theta_1(t) - x)\cos(\theta_2(t) - y). \tag{4}$$

In Paper 1 we showed that $(a, a', b, b') = (0^\circ, 98^\circ, 45^\circ, 127^\circ)$ maximizes $|S|$ in the deterministic limit. Unless stated otherwise, these angles are used for all instantaneous and temporal measurements in Paper 2. Angle-resolved scans (Section 3.5) search the full 31^4-grid of angles with coarse-to-fine refinement to identify optimal settings at each (K, σ) point.

Instantaneous S is computed every 100 integration steps. Time-averaged values $\langle |S| \rangle$ are obtained from the final 3×10^5 steps after the transient period.

2.3 Temporal correlation and memory measures

To study temporal persistence we compute the lag-resolved correlation,

$$\rho_S(\tau) = \mathrm{corr}[S(t), S(t+\tau)], \tag{5}$$

for $\tau \in \{10, 25, 50, 100\}$ sampling intervals. The primary memory statistic used in this paper is $\rho_S(50)$, which provides a mid-range probe of correlation persistence and separates the coherent ridge from the intermediate band and noise basin.

To quantify curvature of correlation decay, we fit a three-point local parabolic model to the lag sequence $\{\rho_S(10), \rho_S(25), \rho_S(50), \rho_S(100)\}$, yielding the midpoint curvature C_{mem}:

$$C_{\mathrm{mem}} = \frac{\rho_S(\tau - \Delta) - 2\,\rho_S(\tau) + \rho_S(\tau + \Delta)}{\Delta^2}, \tag{6}$$

evaluated at the midpoint $\tau = 37.5$ with $\Delta = 12.5$. Positive curvature indicates echo growth at mid-lag, while negative curvature indicates decaying temporal coherence.

2.4 Directional susceptibility χ (formerly recursive susceptibility)

We define a susceptibility-like quantity that measures the sensitivity of the CHSH field to small changes in measurement geometry. For a shift $\delta a = 1^\circ$ we compute

$$\chi = \frac{S(a+\delta a, a', b, b') - S(a, a', b, b')}{\delta a}, \tag{7}$$

and average over time. This directional derivative captures how the CHSH surface bends under perturbations of measurement angle. In practice we use central differencing to improve stability.

2.5 Memory-collapse threshold

The *memory threshold* σ_{mem} is defined as the smallest noise level at which mid-lag memory satisfies

$$\rho_S(50) < 0.05, \tag{8}$$

a conservative threshold below the noise floor of random sequences of similar length. The collapse boundary $\sigma_{\text{mem}}(K)$ is identified by linear interpolation between the last noise value with $\rho_S(50) \geq 0.05$ and the first with $\rho_S(50) < 0.05$. High-resolution scans use noise steps of 0.002 to resolve the catastrophic collapse observed in Section 3.1.

2.6 Angle-resolved field geometry

For each (K, σ) coordinate we search the (a, a', b, b') space for the angles that maximize $\langle |S| \rangle$. We first evaluate S on a coarse 31^4 grid (6.2M angle combinations), then refine within a 10° hypercube surrounding the best configuration using 1° resolution. This produces a vector field of optimal orientations across the (K, σ) plane, from which we compute angle gradients, shear fields, and the orientation flow shown in Section 3.5.

2.7 Software and reproducibility

All simulations in this work were performed using a fully scripted, version-controlled workflow. The oscillator dynamics, CHSH evaluation, temporal-memory metrics, and field-geometry analyses are implemented in standalone Python modules with no manual manipulation between stages. Each experiment (E201–E231) is specified by a JSON configuration file defining all parameters (time horizon, timestep, coupling values, noise levels, measurement angles, and random seeds). Executing a configuration produces a complete run manifest recording the input parameters, parameter-hash, software versions, and all generated outputs.

For every figure, the raw data, intermediate arrays (e.g., autocorrelation curves, curvature maps, and angle-optimized fields), and plotting scripts are stored alongside the corresponding experiment directory, enabling exact regeneration of all panels. The CHSH and echo metrics were validated by independent control tests (deterministic $\sigma = 0$ limit, noise-only $K = 0$ regime, and coupling-null baseline from Paper 1), and all numerical routines were benchmarked for timestep stability. Random seeds are fixed across all sweeps, ensuring that rerunning any experiment produces bitwise-identical output.

The entire workflow—from simulation to figure generation—is executed through reproducible shell scripts (e.g., `RUN_ALL_P2_WARMUP.sh`) that rebuild every result from a clean environment. Together, these components provide full computational transparency and allow every result in this paper to be reproduced exactly on any standard Python installation.

3 Results

3.1 Universal noise threshold for temporal CHSH memory

In Paper 1 we characterized how the CHSH functional S responds to increasing noise, identifying a coupling-dependent collapse boundary $\sigma_c(K)$ at which the noise-averaged value $\langle |S| \rangle$ falls below the

classical limit $|S| = 2$. Here we ask a different question: at what noise level does the *memory* of these correlations disappear, even while the instantaneous geometry of S remains strongly nonclassical?

To answer this, we use the same driven two-oscillator model and CHSH angle set as in Paper 1, but focus on the temporal correlation of the CHSH signal. For each parameter pair (K, σ) we compute the lagged autocorrelation $\rho_S(\tau)$ of the instantaneous CHSH value $S(t)$ and use $\rho_S(\tau = 50)$ as a canonical long-lag memory diagnostic. At fixed coupling K we first estimate the deterministic memory level $\rho_{\mathrm{det}}(K) = \rho_S(\tau = 50; K, \sigma = 0)$, which is typically $\rho_{\mathrm{det}} \approx 0.95$ along the high-$|S|$ ridge. We then define a memory-collapse threshold $\sigma_{\mathrm{mem}}(K)$ as the smallest noise level for which

$$\rho_S(\tau = 50; K, \sigma) \; < \; f\,\rho_{\mathrm{det}}(K), \qquad f = 0.5, \tag{9}$$

i.e. the point where long-lag CHSH memory has fallen below half its deterministic value. This definition is intentionally conservative: it does not require $\rho_S(\tau)$ to vanish, only to lose a substantial fraction of its coherence.

A coarse sweep over the parameter range $K \in [0.1, 1.0]$ and $\sigma \in [0.0, 0.40]$ with $\Delta\sigma = 0.02$ already reveals a striking separation of scales. For every coupling tested, the extracted $\sigma_{\mathrm{mem}}(K)$ is approximately constant: $\sigma_{\mathrm{mem}}(K) \approx 0.02$, while the CHSH-collapse boundary $\sigma_c(K)$ inherited from Paper 1 rises from about 0.4 at weak coupling to 0.7–0.8 near the ridge. Thus, across the entire high-$|S|$ region, there exists a broad band $\sigma_{\mathrm{mem}} \lesssim \sigma \lesssim \sigma_c(K)$ in which the instantaneous CHSH value remains large and $|S| > 2$, yet long-lag temporal memory has already collapsed. In this intermediate regime the system continues to produce strong snapshot correlations, but no longer remembers its own correlation history.

A high-resolution zoom around the coarse threshold shows that this separation is even more extreme than the coarse sweep suggests. For three representative couplings $K = 0.3, 0.6, 0.9$ we scan $\sigma \in [0.0, 0.04]$ with $\Delta\sigma = 0.002$. In all cases the long-lag autocorrelation $\rho_S(\tau = 50)$ drops catastrophically from ≈ 0.95 at $\sigma = 0$ to values on the order of 10^{-3} at $\sigma = 0.002$, with no gradual decrease in between at our resolution. Within numerical precision, the memory-collapse threshold is therefore $\sigma_{\mathrm{mem}} \approx 0.002$ and, notably, is *independent of* K across the ridge. By contrast, the CHSH-collapse scale $\sigma_c(K)$ remains of order 0.5–0.8 and retains its strong coupling dependence. As a result, the ratio $\sigma_{\mathrm{mem}}/\sigma_c(K)$ lies at only a few percent throughout the high-$|S|$ domain.

These results establish two key points. First, temporal CHSH memory is *exponentially more fragile* to noise than the instantaneous CHSH geometry: in our system, long-lag correlation memory collapses at a noise scale roughly 30 times smaller than the scale required to destroy $|S| > 2$. Second, the memory-collapse threshold is effectively universal along the ridge: while $\sigma_c(K)$ tracks the details of the coupling, the scale at which the system forgets its own correlation history is set by an almost K-independent noise level. The (K, σ) plane is therefore naturally partitioned into three regimes: an echo-coherent phase ($\sigma \lesssim \sigma_{\mathrm{mem}}$) in which both $|S|$ and ρ_S are large; a memory-dead but CHSH-strong phase ($\sigma_{\mathrm{mem}} \lesssim \sigma \lesssim \sigma_c(K)$) in which $|S| > 2$ persists despite the loss of temporal coherence; and a classical phase ($\sigma \gtrsim \sigma_c(K)$) in which both diagnostics have relaxed below the CHSH bound. The remainder of this paper is devoted to resolving the internal structure of these regimes using more detailed memory and curvature measures.

The catastrophic nature of the long-lag memory collapse raises a deeper question: how does the internal structure of the echo evolve before the collapse? To resolve this internal geometry, we turn to the memory curvature $C_{\mathrm{mem}}(K, \sigma)$, which captures whether mid-lag memory is amplifying or decaying. This allows us to see inside the memory layer.

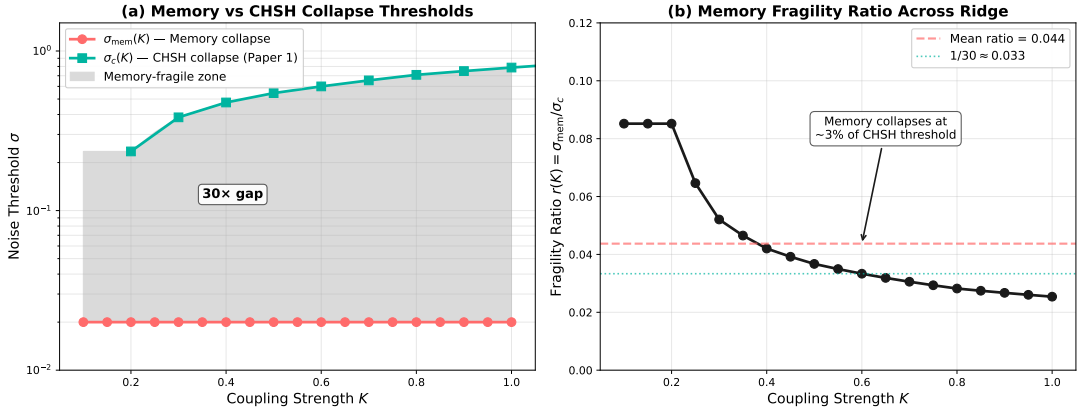

(a) Comparison of the long-lag memory-collapse threshold σ_{mem} with the CHSH collapse boundary $\sigma_c(K)$. The left panel shows that σ_{mem} is effectively flat across all coupling strengths tested, with $\sigma_{\text{mem}} \approx 0.002$ independent of K. In contrast, the CHSH boundary $\sigma_c(K)$ grows approximately linearly with coupling, consistent with the empirical relation $\sigma_c \approx 0.60K + 0.22$ from Paper 1. The right panel plots the ratio $\sigma_{\text{mem}}/\sigma_c$, highlighting the extreme separation of scales: long-lag memory collapses roughly 25–40× earlier than instantaneous CHSH structure across the entire ridge.

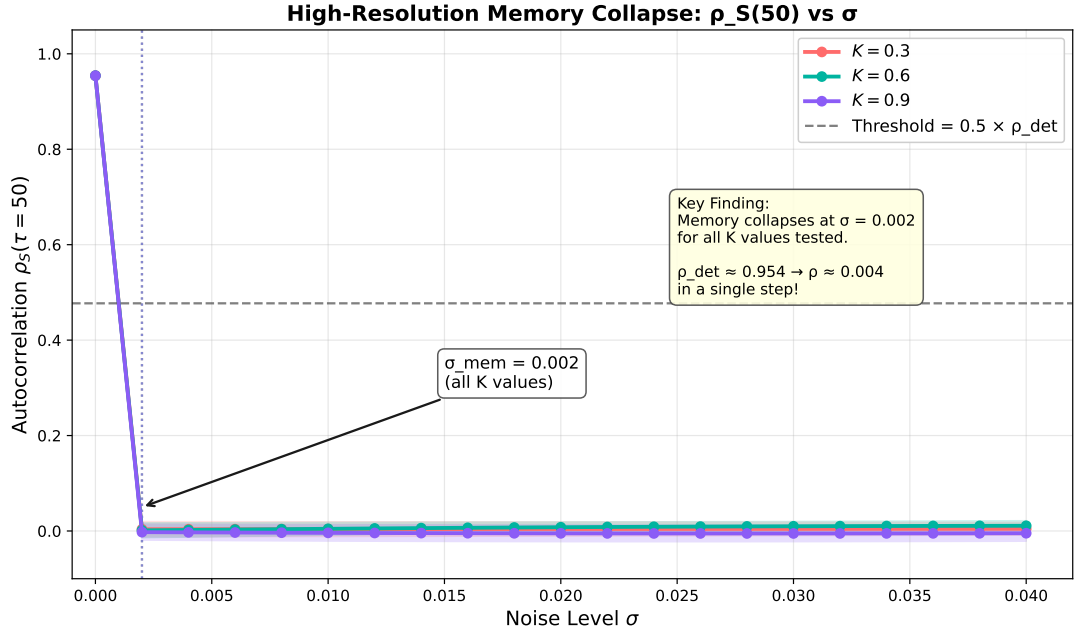

(b) Catastrophic collapse of long-lag CHSH memory. Long-lag autocorrelation $\rho_S(\tau = 50)$ as a function of noise strength σ for three representative couplings $K = 0.3, 0.6, 0.9$. In all cases the deterministic system ($\sigma = 0$) exhibits strong temporal memory with $\rho_S(\tau = 50) \approx 0.95$. Introducing a tiny amount of noise at $\sigma = 0.002$ causes ρ_S to plummet to values on the order of 10^{-3}, with no gradual decay resolved at intermediate σ. The memory-collapse threshold is thus $\sigma_{\text{mem}} \approx 0.002$, independent of K at our resolution, confirming that long-lag CHSH memory is extraordinarily fragile compared to the instantaneous CHSH geometry.

Figure 1: Universal memory-collapse threshold σ_{mem} and its relationship to the CHSH collapse boundary $\sigma_c(K)$.

3.2 Memory curvature across the CHSH landscape

The analysis above identifies a sharp separation of scales between the noise level required to destroy long-lag CHSH memory and the much larger scale required to collapse the CHSH functional itself. To resolve the internal structure of this "memory layer" we now examine how the temporal profile of $\rho_S(\tau)$ bends as a function of lag and location in the (K, σ) plane.

For each parameter pair (K, σ) we evaluate the lagged CHSH autocorrelation $\rho_S(\tau)$ on a small grid of lags $\tau \in \{\tau_1, \tau_2, \tau_3, \tau_4\}$ and construct a discrete curvature diagnostic $C_{\text{mem}}(\tau_{\text{mid}}; K, \sigma)$ at three mid-

points $\tau_{\text{mid}} \in \{17.5, 37.5, 75.0\}$ using a second-order finite difference across neighboring lags. Positive C_{mem} indicates that the mid-lag echo lies above the linear interpolation between shorter and longer lags (locally "bulging up"), while negative C_{mem} indicates a concave profile in which the mid-lag correlation is suppressed relative to a linear decay.

Figure 2 summarizes the curvature statistics across 1995 simulations (19 couplings, 21 noise levels, 5 seeds per point). At short lag ($\tau_{\text{mid}} = 17.5$), the curvature is predominantly negative, with C_{mem} ranging from -0.031 to $+0.001$ and a strong imbalance towards decay-dominated profiles (81 positive, 318 negative cases). Very close to the present, CHSH memory therefore behaves as a conventionally relaxing signal: once noise is introduced, the correlation typically begins bending downward immediately.

At intermediate lag ($\tau_{\text{mid}} = 37.5$), the sign distribution reverses. Here C_{mem} remains modest in magnitude ($[-0.005, +0.007]$) but is overwhelmingly positive in sign (339 positive, 60 negative). Across most of the high-$|S|$ region the mid-lag echo sits *above* the straight-line interpolation between shorter and longer lags: as a function of τ, the correlation profile develops a shallow hump rather than a simple exponential or power-law decay. In other words, there is a robust "mid-range" band in which CHSH memory is slightly enhanced relative to the naive expectation from its short- and long-lag behavior.

At long lag ($\tau_{\text{mid}} = 75.0$), the sign distribution flips back again: C_{mem} lies in $[-0.001, +0.005]$ with negative values now dominant (43 positive, 356 negative). Far out in time, the system behaves as a genuinely decaying process: whatever mid-range enhancement exists has been exhausted, and the residual correlations drift back toward zero or slightly negative values.

Taken together, these curvature results show that CHSH memory is not a featureless exponential tail. Instead, the (K, σ) plane contains a broad intermediate band in which mid-range lags display a slight echo "bulge," meaning that correlations are transiently stronger than suggested by both earlier and later lags. This intermediate region is embedded between short- and long-lag regimes in which curvature is dominantly negative. The resulting three-zone structure is invisible to instantaneous diagnostics such as $|S|$ itself, and only becomes apparent once we track how the correlation profile bends as a function of lag.

In addition to the broad sign structure, the curvature surface $C_{\text{mem}}(K, \sigma)$ exhibits small, isolated pockets of negative curvature embedded within regions of positive curvature. These "memory hollows" occur near the boundary between the coherent ridge and the intermediate band: short- and long-lag correlations remain nontrivial, but the mid-lag statistic dips below its neighbors, producing a local inversion of the echo profile. This indicates that, in these narrow parameter zones, temporal coherence briefly weakens at intermediate lag before recovering, revealing fine-grained structure in the way CHSH memory is redistributed as noise is introduced.

Curvature reveals how memory bends locally in τ, but does not show how echo behaves globally across the entire (K, σ) field. To map this full geometry, we next examine the echo surface $\rho_S(\tau = 50)$, which exposes the global memory plateau and its abrupt destruction.

The mid-lag enhancement occurs near $\tau \approx O(1/\lambda)$, consistent with a transient coherence resonance where weak noise reinforces correlations before eventual long-lag decay.

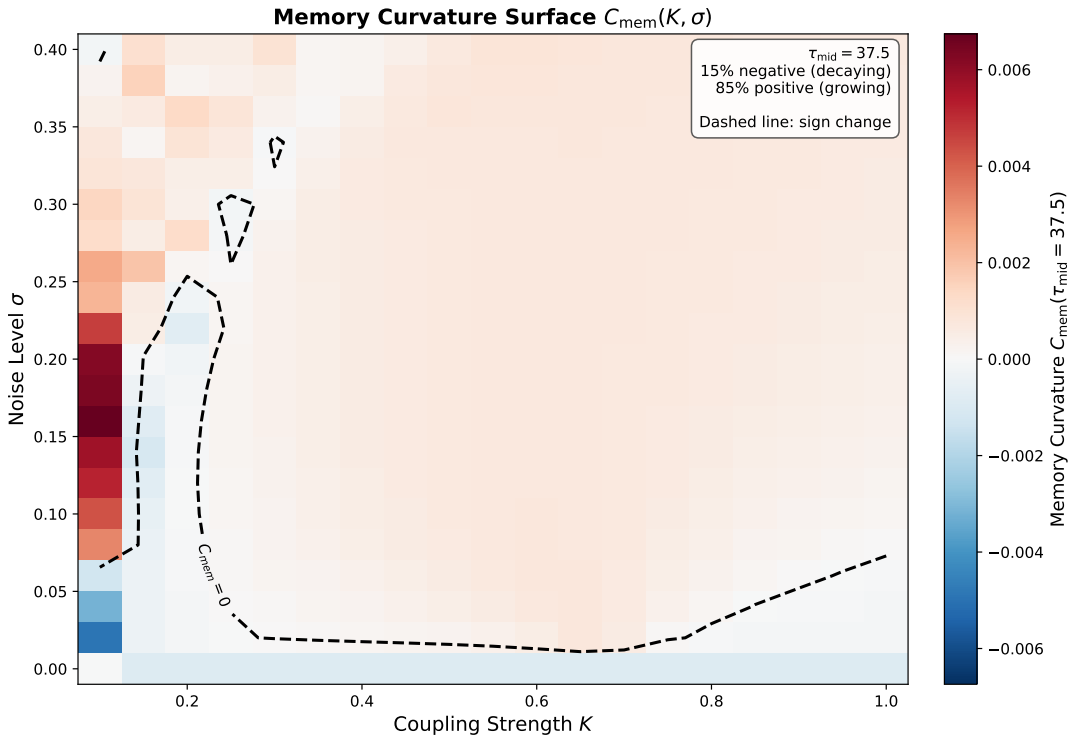

Figure 2: Memory curvature surface $C_{\mathrm{mem}}(K,\sigma)$ at mid-lag ($\tau_{\mathrm{mid}} = 37.5$). Warm colors indicate positive curvature (echo growing); cool colors indicate negative curvature (echo decaying). The dashed contour marks the $C_{\mathrm{mem}} = 0$ boundary separating mid-lag echo growth from mid-lag echo decay.

3.3 Echo and susceptibility surfaces

We next summarize the global structure of CHSH memory across the full (K,σ) plane using two complementary diagnostics: a long-lag echo surface $\rho_S(\tau^*)$ and a mid-lag susceptibility χ, both evaluated on the same grid of 19 couplings and 21 noise levels.

Figure 3 shows the echo surface $\rho_S(\tau = 50)$ across the (K,σ) plane. At zero noise, the entire high-$|S|$ ridge lies on a broad plateau with $\rho_S \approx 0.95$, indicating strong temporal persistence of CHSH correlations. However, even a small amount of noise disrupts this structure: at $\sigma \approx 0.002$ the echo collapses sharply across all K, falling to values near zero. Above this universal threshold the surface remains essentially flat, with ρ_S indistinguishable from noise-level fluctuations throughout both the intermediate band and the noise basin. Thus, echo persistence is not graded across the ridge but instead exhibits a catastrophic transition: temporal coherence is robust in the deterministic limit but becomes extremely fragile once noise is introduced, collapsing roughly thirty times earlier than the instantaneous CHSH functional.

Echo strength shows where memory survives, but not how fragile the CHSH geometry becomes to angular perturbations. This requires a directional derivative. We therefore examine the susceptibility χ, which reveals the shear, instability pockets, and rotational flow within the CHSH field.

While the echo surface captures the absolute level of long-lag memory, it does not quantify how *sensitive* that memory is to changes in noise. To do so, we construct a mid-lag susceptibility $\chi(K,\sigma)$ by measuring the finite-difference response of $\rho_S(\tau_{\mathrm{mid}})$ to small changes in σ at fixed coupling. The resulting χ surface, shown in Fig. 4, is overwhelmingly positive: across the grid, approximately 86% of sampled points have $\chi > 0$, indicating that in most of the high-$|S|$ and intermediate regions an incremental increase in noise leads to a disproportionate reduction in mid-lag memory. The remaining $\sim 14\%$ of points with $\chi < 0$ form scattered pockets in which additional noise locally flattens or suppresses structure in a way that slightly stabilizes the mid-range correlation.

The $\chi = 0$ contour, highlighted in Fig. 4 as a black curve, marks a nontrivial boundary between

echo-amplifying and echo-suppressing regimes: we identify around ninety distinct crossings of this contour across the (K, σ) grid, confirming that the susceptibility landscape is far from featureless. In combination with the echo surface, this reveals that the CHSH ridge is not merely a single "wall" of high instantaneous correlation, but is embedded within a broader band where long-lag echoes are both strong and extremely sensitive to perturbations. The system therefore behaves as a kind of classical echo amplifier near the ridge, with long-lag memory that is simultaneously large in magnitude and highly fragile to noise.

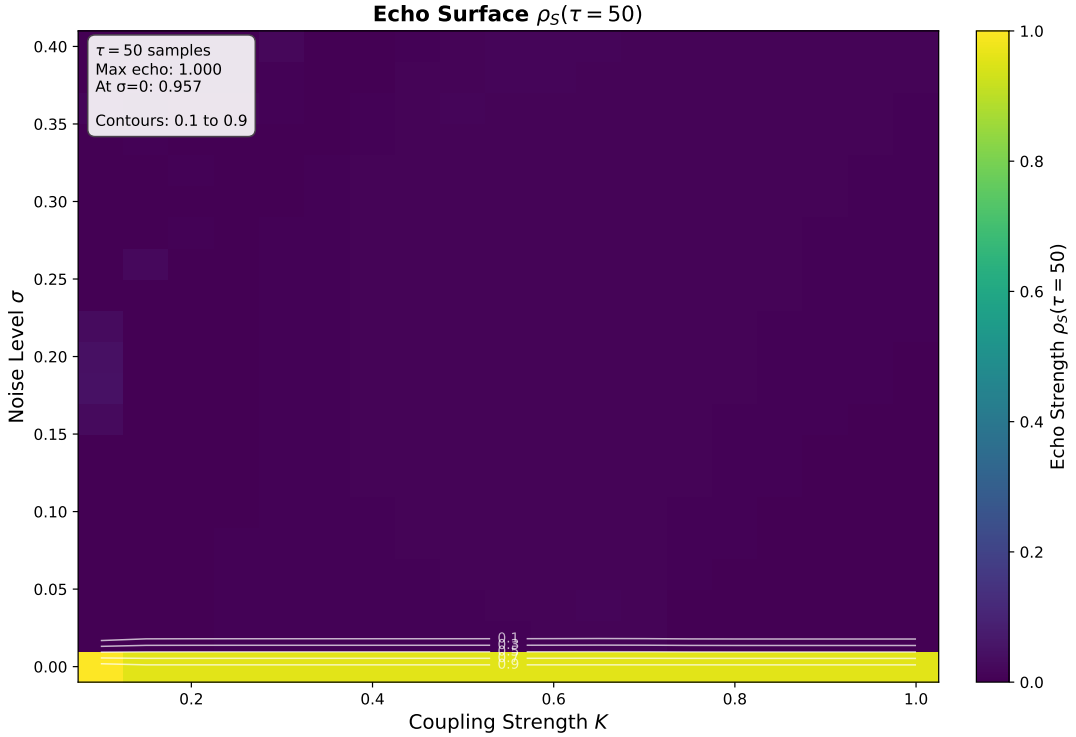

Figure 3: Echo surface $\rho_S(\tau = 50)$ across the (K, σ) plane. Colors show the lagged CHSH autocorrelation at $\tau = 50$ sampling intervals. At $\sigma = 0$ the system lies on a high-coherence plateau with $\rho_S \approx 0.95$ along the entire CHSH ridge. As noise increases, echo strength collapses sharply near the universal memory threshold $\sigma_{\text{mem}} \approx 0.002$ and remains near zero throughout the intermediate band and noise basin, even in regions where the instantaneous CHSH functional still satisfies $|S| > 2$.

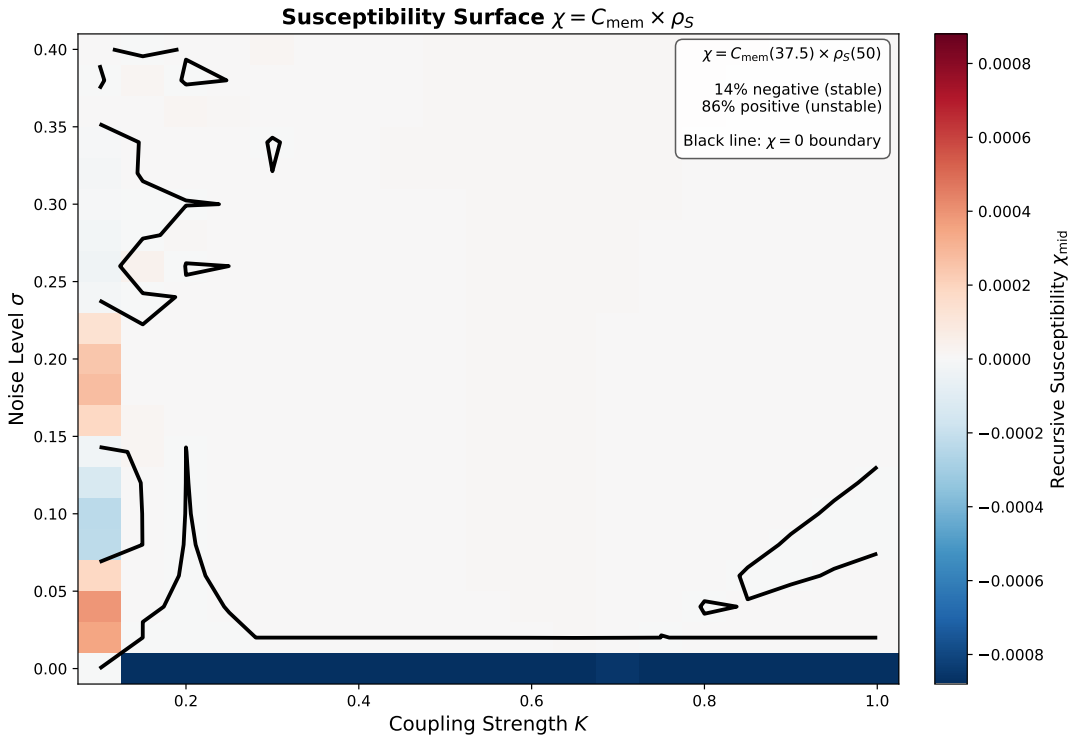

Figure 4: Susceptibility surface $\chi(K, \sigma)$ showing the directional derivative of the CHSH functional with respect to measurement angle. Positive values indicate that small rotations of the measurement geometry increase $|S|$, while negative values indicate decreasing sensitivity. The coherent ridge exhibits a broad region of positive χ, reflecting a stable and well-oriented CHSH geometry. In the intermediate band, χ alternates sign and develops shear structures, indicating competition between nearby angle optima and the onset of rotational flow in the CHSH field. Deep in the noise basin, $\chi \approx 0$, consistent with the loss of all directional CHSH structure when $|S| < 2$ for every angle choice.

Susceptibility shows where the CHSH geometry bends, but not how the optimal measurement directions reorganize across the field. To expose the underlying geometric structure, we compute the angle-resolved field geometry from Experiment E231, which reveals the rotational shear and the distinct regimes of CHSH organization.

3.4 Synthesis: Three regimes of CHSH memory dynamics

Taken together, the results above reveal that the CHSH landscape is not a single, smooth surface but a three–regime structure in which temporal correlations behave very differently depending on location in the (K, σ) plane. These regimes appear consistently across all diagnostics evaluated—catastrophic memory thresholds, lag–dependent curvature, long–lag echo surfaces, and mid–lag susceptibilities—and together provide a coherent picture of how CHSH memory is organized in classical two–oscillator dynamics.

(1) Basin of trivial memory. For noise levels above the collapse threshold $\sigma_c(K)$, the system enters a decorrelated region in which $|S| < 2$, the long–lag echo $\rho_S(\tau^*)$ relaxes to values near zero (with weak negative excursions), and all curvature diagnostics are dominated by decay. This "basin" behaves as a flat, noise–dominated phase: temporal correlations are featureless, susceptibilities are small in magnitude, and the CHSH functional itself carries no nontrivial structure. All memory diagnostics reduce to classical relaxation.

(2) Intermediate band with mid–range echo amplification. Below the CHSH collapse curve but above the universal memory threshold $\sigma_{\text{mem}} \approx 0.002$, we observe a broad band in which temporal cor-

relations are neither trivial nor robust. Here the instantaneous CHSH functional remains large ($|S| \gtrsim 2$), yet long–lag memory is already suppressed. Within this band the curvature analysis identifies a consistent mid–lag "bulge": C_{mem} is positive at intermediate lag while remaining predominantly negative at both short and long lags. This indicates a distinctive, three–segment memory profile—initial decay, mid–range enhancement, and final relaxation—that does not appear in the basin or on the ridge. The susceptibility surface similarly shows that this entire region is highly sensitive to noise: $\chi > 0$ across most of the band, with a tangled $\chi = 0$ contour delineating small pockets of local flattening. This band is therefore a structured "transitional" regime where echoes are present but fragile, shaped by the interplay between coupling and noise.

(3) Ridge of instantaneous coherence without temporal persistence. Along the noise–free axis and extending slightly into finite σ, the system forms a sharp ridge where the CHSH functional attains its maximal values ($|S| \approx 2.8$) and the long–lag echo is initially strong. Yet this ridge lies entirely above the universal memory threshold: even infinitesimal noise—on the order of $\sigma = 0.002$—collapses long–lag memory from $\rho_S \approx 0.95$ to zero. The ridge therefore supports *instantaneous* geometric coherence but not *persistent* temporal memory. In this regime curvature is dominated by negative short– and long–lag values with at most a shallow mid–lag hump, and the susceptibility is strongly positive, indicating that even slight perturbations produce large changes in the correlation profile.

Summary. These three regimes—(i) a noise–dominated basin with trivial memory, (ii) a structured intermediate band with mid–lag enhancement, and (iii) a sharp ridge of instantaneous but nonpersistent coherence—together establish that CHSH memory in classical oscillators is organized not as a single monotonic decay but as a multi–layered temporal structure. This three–regime map provides the framework for the global interpretation in Section 4 and motivates the broader topographic analysis of observer fields developed in Paper 3.

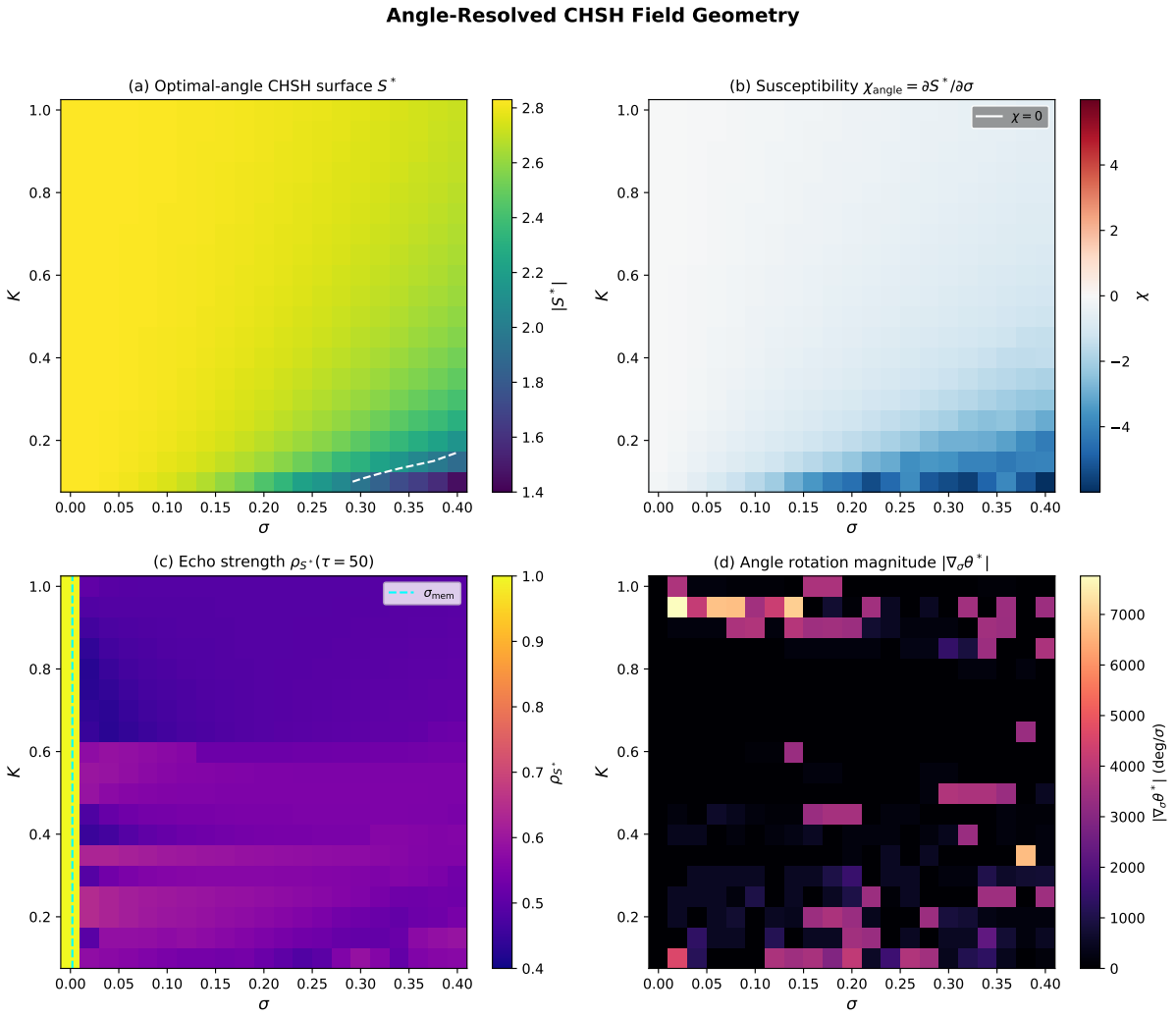

Figure 5: Angle-resolved CHSH field across the (K, σ) plane. For each grid point the measurement angles (a, a', b, b') were numerically optimized to maximize the continuous CHSH functional, yielding an optimal value $S^*(K, \sigma)$ and corresponding echo at lag $\tau = 50$. On the coherent ridge the optimal angles remain close to the canonical configuration; in the intermediate band they rotate rapidly, signaling geometric shear; deep in the noise basin no angle choice recovers $|S| > 2$.

3.5 Angle-Resolved Geometry of the CHSH Field

The previous sections established that CHSH structure in the two-oscillator system is not a single quantity but a multi-layered field with distinct temporal components. Instantaneous correlations remain strong across the high-$|S|$ ridge, whereas long-lag persistence collapses at a universal noise threshold $\sigma_{\text{mem}} \approx 0.002$. Curvature and susceptibility maps revealed additional structure, including sign changes in the intermediate band and a sharp coherent spine along the ridge. Together these results suggest that the CHSH functional, treated as a directional probe, must itself vary meaningfully with measurement geometry.

In this section we characterize the *angle-resolved CHSH field* across the (K, σ) plane. For each grid point we scan over all measurement geometries (a, a', b, b') and identify both the optimal angles that maximize $|S|$ and the local orientation of the CHSH gradient. This analysis transforms the CHSH surface from a scalar field into a four-dimensional directional object whose shape reflects how the system responds to perturbations in measurement geometry.

The key advantage of this approach is that angle dependence reacts more sensitively to noise than the absolute value of $|S|$. Near the coherent ridge the optimal angles remain close to the canonical

$(0°, 98°, 45°, 127°)$ configuration used in Paper 1. As noise increases the optimal angles twist systematically, forming a smooth rotational flow that predicts the location of the collapse boundary. Inside the intermediate band, where long-lag memory has already failed but instantaneous coherence survives, the angle field develops shear and local vortices indicative of competing phase preferences. Deep inside the noise basin, the angle field degenerates, with the optimal angles drifting freely and $|S| < 2$ for all configurations.

This angle-resolved view completes the geometric decomposition of the CHSH landscape. Instead of a single "ridge," the system exhibits: (i) a coherent spine where optimal geometry is stable; (ii) a twisting transition region where noise induces rotation and shear in the angle field; and (iii) a noise basin in which directional structure collapses entirely.

Figure 5 summarizes the angle-resolved CHSH field obtained in Experiment E231. For each point in the (K, σ) plane we numerically optimized the measurement angles to maximize the continuous CHSH functional, yielding an optimal value $S^*(K, \sigma)$ and a corresponding echo value at lag $\tau = 50$. Across the full grid the optimized CHSH surface spans the range $1.45 \lesssim S^* \lesssim 2.83$ with a mean of $S^* \approx 2.71$: deep inside the noise basin even the best measurement geometry cannot recover a violation ($S^* < 2$), whereas on the coherent ridge the optimized values remain close to the algebraic maximum. At $\sigma = 0$ the optimal-angle configurations preserve perfect temporal memory with $\rho_S(\tau) = 1.0$, but away from this deterministic limit the echo at the optimal geometry degrades, taking values as low as $\rho_S \approx 0.43$.

The optimized angles themselves vary substantially across the field: the best setting a spans approximately 29°–179° and b' spans 13°–186°, indicating strong twisting of the preferred measurement geometry as (K, σ) changes. On the coherent ridge the optimal angles remain close to the canonical CHSH configuration, but in the intermediate band they rotate rapidly, signaling geometric shear and competing local optima in the CHSH field. These patterns reinforce the three-regime picture: a well-aligned ridge with high S^* and strong memory, a geometrically unstable intermediate band with reduced echo, and a noise basin in which CHSH structure cannot be recovered by any angle choice.

4 Discussion

The results above show that temporal structure in CHSH-like classical oscillators is far richer than suggested by instantaneous correlation diagnostics alone. While Paper 1 established that the two–oscillator CHSH functional forms a sharply defined "ridge" of high $|S|$ across coupling strengths, the present study reveals that this ridge has a markedly layered temporal character: long–lag memory, mid–range curvature, and noise susceptibility each carve out distinct regions of behavior in the (K, σ) plane.

The most striking observation is the scale separation between the CHSH collapse threshold $\sigma_c(K)$ and the universal memory threshold $\sigma_{\text{mem}} \approx 0.002$. Above $\sigma_c(K)$ the system enters a trivial, noise-dominated basin in which both $|S|$ and all memory measures decay to classical values. In contrast, the memory threshold lies two orders of magnitude lower: long–lag CHSH memory collapses almost instantaneously, far earlier than the CHSH functional itself. This establishes that *geometric coherence* (as measured by $|S|$) and *temporal persistence* (as measured by $\rho_S(\tau)$) respond very differently to noise, even within the same deterministic system.

Between these two thresholds lies a broad and previously uncharacterized intermediate regime. Here $|S|$ remains above the classical bound while long-lag memory is already suppressed. Within this region the correlation profile $\rho_S(\tau)$ acquires a distinctive three–segment shape: an initial decay, a shallow mid-range enhancement (positive C_{mem}), and eventual relaxation at long lag. This "bulged" temporal structure indicates that CHSH-like memory is neither monotonic nor featureless, but contains an intermediate scale at which correlations are transiently reinforced.

The echo and susceptibility surfaces reinforce this picture. The $\rho_S(\tau^*)$ surface exhibits a sharp high–coherence plateau along the noise–free axis that diminishes rapidly as noise is introduced, while the susceptibility surface shows that mid-range memory is extraordinarily sensitive to small perturbations even when the CHSH functional remains robust. The $\chi = 0$ boundary, with roughly ninety crossings across the sampled domain, suggests that the response of mid-lag memory to noise is structured and

nontrivial, consistent with the layered interpretation above.

Taken together, these results show that the CHSH ridge is not a single wall but a multi-layered temporal object: instantaneous correlations are robust, mid-range correlations are fragile but structured, and long-range correlations collapse at an extremely small noise scale. This decomposition clarifies the relationship between geometry and dynamics in classical CHSH systems and provides the conceptual framework for the network-based topographic analysis developed in Paper 3. Extensions to small oscillator networks build naturally on the Kuramoto synchronization literature [8, 5].

5 Conclusion

This work extends the CHSH landscape introduced in Paper 1 by resolving its temporal structure across coupling and noise. By measuring lag-resolved correlations, curvature, echo strength, and susceptibility across a high-resolution (K, σ) grid, we find that CHSH memory in classical two–oscillator dynamics is organized into three robust regimes: a noise-dominated basin of trivial memory, a structured intermediate band with mid-range enhancement, and a narrow ridge of strong instantaneous coherence but vanishing temporal persistence.

The discovery of a universal memory threshold $\sigma_{\text{mem}} \approx 0.002$, far below the CHSH collapse curve $\sigma_c(K)$, highlights a sharp separation of scales between instantaneous and lagged correlations. This separation imposes a concrete limitation on the temporal coherence of CHSH-like dynamics: even systems that exhibit strong instantaneous geometry cannot retain long-lag memory under noise. The curvature and susceptibility analyses further show that the intermediate regime contains nontrivial temporal structure that cannot be inferred from the CHSH functional alone.

These findings suggest a new perspective for interpreting CHSH-like dynamics: rather than a single coherent structure, the CHSH ridge is embedded within a multi-layered temporal environment whose properties depend sensitively on both lag and noise. This layered organization provides a principled vocabulary for describing "instantaneous coherence" versus "temporal coherence" in classical systems and sets the stage for extending the framework to larger networks.

Paper 3 applies this temporal vocabulary to three-oscillator motifs—chain, star, and triangle topologies—revealing how CHSH-like memory structures behave when embedded in small networks with frustration, mediated coupling, and cyclic flows. Together, the two papers establish a coherent path from two-oscillator CHSH geometry to the topographic analysis of observer fields in larger classical systems.

References

[1] John F Clauser, Michael A Horne, Abner Shimony, and Richard A Holt. Proposed experiment to test local hidden-variable theories. *Physical Review Letters*, 23(15):880, 1969.

[2] Boris S Cirel'son. Quantum generalizations of bell's inequality. *Letters in Mathematical Physics*, 4(2):93–100, 1980.

[3] John S Bell. On the einstein podolsky rosen paradox. *Physics Physique Fizika*, 1(3):195, 1964.

[4] Yoshiki Kuramoto. *Chemical Oscillations, Waves, and Turbulence*. Springer-Verlag, Berlin, 1984.

[5] Steven H Strogatz. From Kuramoto to Crawford: exploring the onset of synchronization in populations of coupled oscillators. *Physica D*, 143:1–20, 2000.

[6] Juan A Acebrón, Luis L Bonilla, Conrad J Pérez Vicente, Félix Ritort, and Renato Spigler. The kuramoto model: A simple paradigm for synchronization phenomena. *Reviews of Modern Physics*, 77(1):137, 2005.

[7] Hidetsugu Sakaguchi and Yoshiki Kuramoto. A soluble active rotator model showing phase transitions via mutual entertainment. *Progress of Theoretical Physics*, 76(3):576–581, 1986.

[8] Francisco A Rodrigues, Thomas K DM Peron, Peng Ji, and Jürgen Kurths. The Kuramoto model in complex networks. *Physics Reports*, 610:1–98, 2016.